

Formation of N-Heterocyclic Carbene–Boryl Radicals through Electrochemical and Photochemical Cleavage of the B–S bond in N-Heterocyclic Carbene–Boryl Sulfides

Sofia Telitel,[†] Anne-Laure Vallet,[‡] Stéphane Schweizer,[§] Bernard Delpech,[‡] Nicolas Blanchard,[⊥] Fabrice Morlet-Savary,[†] Bernadette Graff,[†] Dennis P. Curran,^{||} Marc Robert,^{*,∇} Emmanuel Lacôte,^{*,#} and Jacques Lalevée^{*,†}

[†]Institut de Science des Matériaux de Mulhouse IS2M (UMR CNRS 7361), Université de Haute Alsace, 15 rue Jean Starcky, 68057 Mulhouse Cedex, France

[‡]ICSN CNRS, Avenue de la Terrasse, 91198 Gif-sur-Yvette Cedex France

[§]Laboratoire de Chimie Organique et Bioorganique (EA 4566), Université de Haute-Alsace-ENSCMu, 3 rue Alfred Werner, 68093 Mulhouse Cedex, France

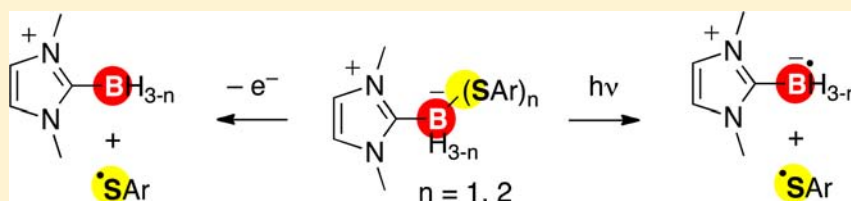
[⊥]Laboratoire de Chimie Moléculaire (UMR CNRS 7509), École Européenne de Chimie, Polymères et Matériaux, Université de Strasbourg, 25 rue Becquerel, 67087 Strasbourg, France

^{||}Department of Chemistry, University of Pittsburgh, Pittsburgh, Pennsylvania 15260 United States

[∇]Laboratoire d'Électrochimie Moléculaire (UMR CNRS 7591), Université Paris Diderot, Sorbonne Paris Cité, 15 rue Jean-Antoine de Baïf, 75013 Paris, France

[#]Institut de chimie de Lyon, Université de Lyon, UMR 5265 CNRS-Université Lyon I-ESCP Lyon, 43 Bd du 11 novembre 1918, 69616 Villeurbanne, France

S Supporting Information



ABSTRACT: The B–S bond in N-heterocyclic carbene (NHC)–boryl sulfides can be cleaved homolytically to NHC–boryl or NHC–thioboryl and thiyl radicals using light, either directly around 300 nm or with a sensitizer at a longer wavelength (>340 nm). In contrast, the electrochemical reductive cleavage of the B–S bond is difficult. This easy photolytic cleavage makes the NHC–boryl sulfides good type I photopolymerization initiators for the polymerization of acrylates under air.

INTRODUCTION

The complexation of boranes by N-heterocyclic carbenes (NHCs) generates stable adducts¹ that can be used as reagents for both organic^{2–5} and polymer synthesis.^{6–10} In radical-based transformations, the rich chemistry of NHC-complexed boryl radicals has found many uses. Such radicals can homolytically substitute mono-^{3,7,11} and divalent¹² atoms, add to xanthates^{2,13} and electron-poor olefins,^{7,9} dimerize,^{14–16} or enter redox processes.^{17–19} In other words, NHC–boryl radicals undergo nearly all of the elementary steps open to carbon-centered radicals and thus have a high synthetic potential.

Previous work on radical, ionic, and organometallic reactions of NHC–boranes has focused almost exclusively on Lewis pairs involving a variety of different NHCs and the parent borane (BH₃). Attention is now shifting to B-substituted NHC–boranes, and new reaction modes are being uncovered. For example, B-alkyl and B-aryl substituents can help stabilize

boreniums,^{19,20} generate frustrated Lewis pairs,²¹ or lead to radical β -eliminations.¹⁴ Also, B-substituents can be transferred to palladium complexes for Suzuki–Miyaura couplings.²² NHC–boryl halides can be reduced by electron transfer to generate boryl anions,^{17,18} borylenes,^{23,24} and multiply bonded diboron compounds.²⁵ And NHC monoadducts of diboranes have a rich chemistry of their own.^{14,26–28}

We have shown that NHC–boranes react with diaryl disulfides to form NHC–boryl mono- and bis-sulfides. NHC–Boryl sulfides are a new family of B-substituted NHC–boranes with unexplored chemistry.¹²

Here we describe the cleavage of the B–S bond in NHC–boryl mono- and bis-sulfides by irradiation with and without photosensitizers and by electrochemical stimulation. The

Received: June 29, 2013

Published: October 10, 2013

resulting reactive intermediates have been characterized by EPR spectroscopy and cyclic voltammetry. To illustrate the use of this easy B–S photolytic cleavage, we investigated NHC–boryl sulfides as type I initiators for the direct and sensitized photopolymerization of acrylates.

RESULTS AND DISCUSSION

The compounds examined in this study were prepared in one step by thermal or photochemical reactions of NHC–boranes with disulfides (Figure 1).¹² Both mono- (**1–10**) and bis-

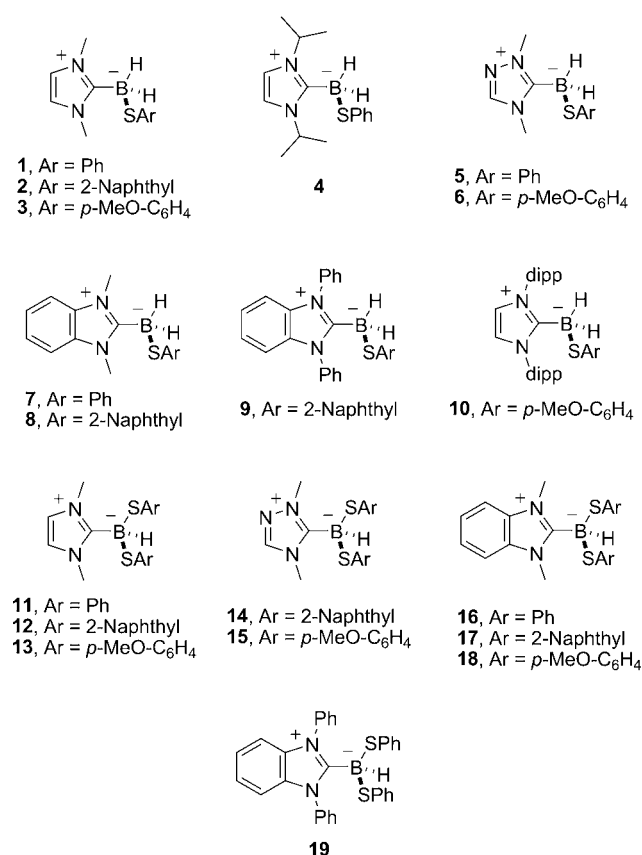


Figure 1. Structures of the NHC–boryl sulfides used in this work.

sulfide complexes (**11–19**) were made with an assortment of substituents on the NHC ring and the sulfide. The NHCs used were the dimethyl- and di-isopropyl-imidazolylidene (as in **1–4** and **11–13**); the bis-di-isopropylphenyl-imidazolylidene (as in **10**); the diphenyl-benzimidazolylidene (as in **9** and **19**); the dimethyl-benzimidazolylidene (as in **7**, **8**, and **16–18**) and the dimethyl-triazolylidene (as in **5**, **6**, **14**, and **15**). The substituents at sulfur were phenyl, 2-naphthyl and *p*-methoxyphenyl.

Photochemical Properties. Light Absorption. A typical UV absorption spectrum of a NHC–boryl monosulfide (**4**) is shown in Figure 2. There is a strong absorption at 268 nm ($\epsilon = 12\,000\text{ M}^{-1}\text{ cm}^{-1}$, Figure 2A, curve a). In contrast, the parent NHC–BH₃ complex does not have this transition, and its light absorption at lower wavelengths is also weaker ($\epsilon < 2000\text{ M}^{-1}\text{ cm}^{-1}$ at 200 nm, Figure 2A, curve c).

Based on molecular orbital calculations, we attribute the absorption band at 268 nm in monosulfide **4** to a charge transfer $\pi \rightarrow \pi^*$ transition from the sulfide to the NHC. The calculated HOMO and LUMO of **4** are depicted in Figure 2B.

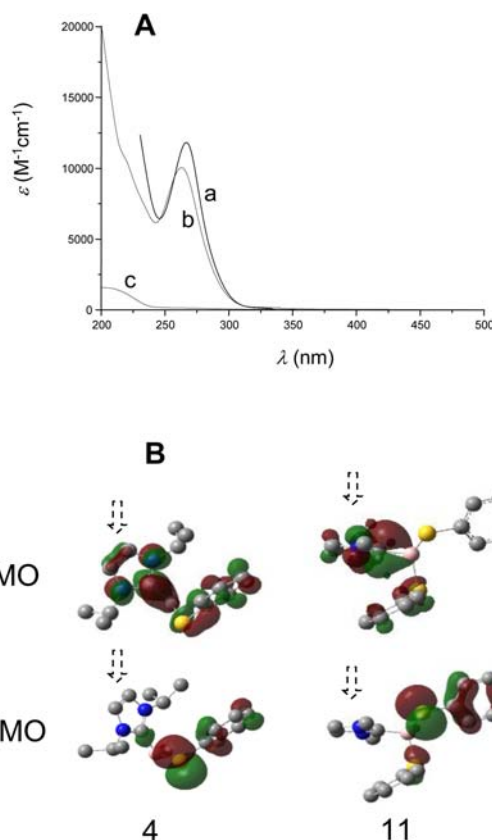


Figure 2. (A) UV absorption spectra for (a) **4**, (b) **11**, and (c) DiMe-Imd–BH₃ and (B) HOMO–LUMO orbitals involved in the $\pi \rightarrow \pi^*$ transition for **4** and **11** (calculated at the UB3LYP/6-31G* level; the NHC is indicated by the dashed arrow; the hydrogen atoms are not shown for clarity).

These orbitals are mainly centered on the thioether and carbene moieties, respectively, suggesting a high charge transfer character for the HOMO–LUMO $\pi \rightarrow \pi^*$ transition. NHC–boryl disulfide **11** exhibited a similar strong absorption at 260 nm (Figure 2A, curve b) and similar calculated frontier orbitals. This suggests a similar HOMO–LUMO transition (Figure 2B).

The measured values for the maximum absorption wavelength, as well as of the ϵ associated with the transitions for 10 NHC–boryl sulfides are reported in Table 1. The maxima all fall into the range of 260–330 nm.

We also calculated the BDEs for the various B–S bonds at the UB3LYP/6-31G* level (Table 1). All calculated BDEs were

Table 1. Absorption Properties in MeCN (λ_{max} , ϵ) and Calculated B–S BDEs (at the UB3LYP/6-31G* Level)

entry	NHCB	λ_{max} (nm)	ϵ (M ⁻¹ cm ⁻¹)	BDE (kcal mol ⁻¹)
1	4	268	12000	60.0
2	5	300	9200	54.8
3	7	270	24600	53.8
4	8	260 (300) ^a	25000	54.3
5	11	263	10500	53.3
6	12	328	4100	51.6
7	13	258	18000	50.3
8	14	300	44000	49.7
9	16	263	21600	49.3
10	17	260 (300) ^a	41000	47.4

^aA shoulder was observed at ~300 nm.

rather low. The highest calculated value was for NHC–boryl monophenylsulfide **4** (60 kcal/mol) and the lowest was for NHC–boryl bis-naphthylsulfide **17** (47.4 kcal/mol).

Since all absorptions observed match well the emission of the practically convenient Xe–Hg light source (see Figure S1 in the Supporting Information), the photochemistry of NHC–boryl sulfides was investigated. The low BDEs (B–S) of the latter suggest that photolysis may result in B–S bond cleavage to form NHC–boryl and thiyl radicals.

Photochemical Reactivity. In a typical photolysis experiment, NHC–boryl monosulfide **5** was irradiated with a Xe–Hg lamp (~ 56 mW/cm²) in acetonitrile. The $\pi \rightarrow \pi^*$ transition band at 300 nm smoothly disappeared over only 40 s (Figure 3B). The band at 263 nm for NHC–boryl bis-sulfide **11** also

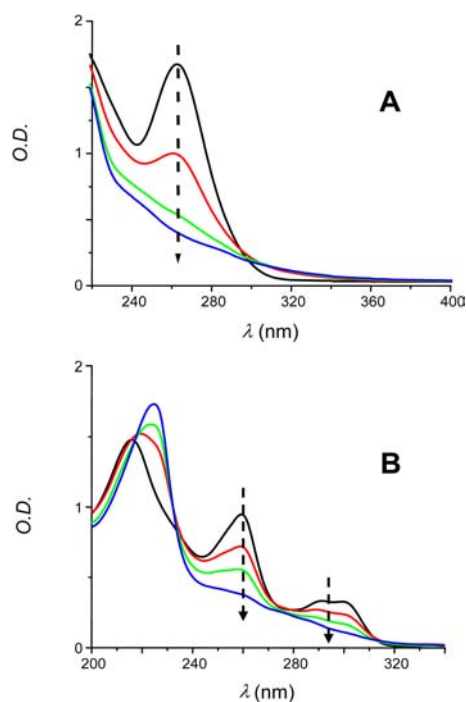


Figure 3. Photolysis of (A) **11** and (B) **5** in acetonitrile upon Xe–Hg lamp exposure from $t = 0$ (black curve) to 40 s (blue curve, intensity ~ 56 mW/cm²).

disappeared over 40 s (Figure 3A). A similar behavior was observed for all NHC–boryl sulfides examined (see the case of **18** in Figure S2, Supporting Information). This strongly suggests that the compounds have a very high photosensitivity.

Electron Spin Resonance (ESR)-Spin Trapping. We conducted ESR-spin trapping experiments with complexes **4**, **5**, **7**, **8**, **11–14**, **16**, and **17** to shed light on the photochemical processes involved. Representative spectra are shown in Figure 4, and further spectra are shown in Figure S3 in the Supporting Information. Standard analysis provided the hyperfine coupling values in Table 2.

In a typical experiment (Scheme 1), a deaerated solution of complex **4** and PBN (*N-tert-butyl- α -phenyl nitron*) in *tert*-butylbenzene was irradiated in the cavity of an ESR spectrometer. The resulting spectrum showed a signal at the g factor characteristic of nitroxide radicals. We assign the spectrum as a superposition of signals from **21**[•] and **22**[•]. The known PhS[•]/PBN radical adduct **22**[•] is characterized by hyperfine coupling constants $a_N = 13.9$ and $a_H = 1.8$ G²⁹ (Figure 4A). The structure of the new nitroxide was assigned as

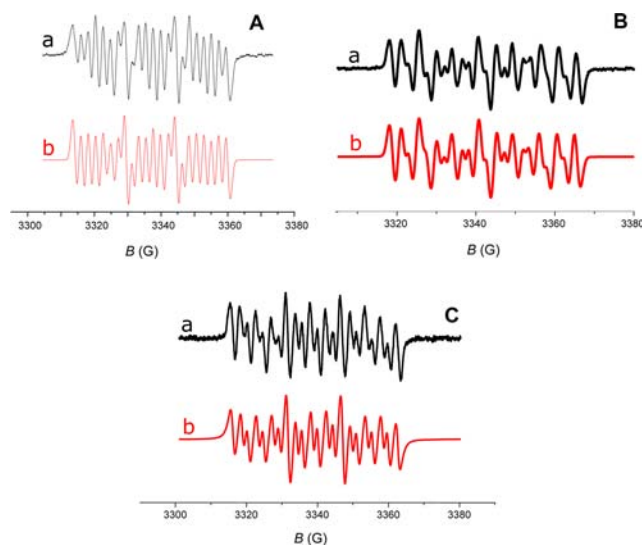


Figure 4. ESR-spin trapping spectra for the irradiation of (A) **4**, (B) **11**, and (C) **12** solutions in *tert*-butylbenzene; [PBN] = 0.01 M; experimental (a, black) and simulated (b, red) spectra.

the NHC boryl/PBN radical adduct **21**[•]. This exhibits three significant hyperfine coupling constants with EPR active nuclei: one ($a_N = 15.1$ G) indicating an α -N atom, a second ($a_H = 2.1$ G) characteristic of a β -H, and a third ($a_B = 4.6$ G) consistent with a β -B atom.^{6,7,9,10,30}

Under the same conditions, NHC–thioboryl adduct **24**[•] (characterized by $a_N = 15.2$, $a_H = 2.7$, and $a_B = 4.4$ G) was observed together with **22**[•] from NHC–boryl bis-sulfide **11** (Figure 4B). On the other hand, the ESR-ST spectrum of NHC–boryl bis-naphthylsulfide **12** showed only the NHC–boryl adduct radical **26**[•] (Figure 4C). The naphthylS[•]/PBN radical adduct **27**[•] was not observed.

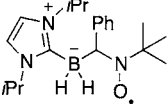
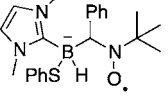
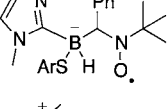
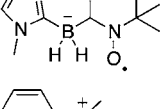
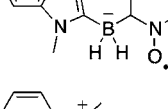
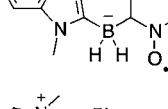
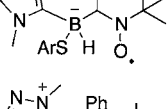
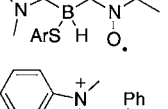
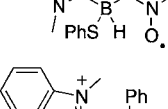
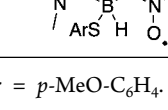
The observation of adducts derived from both B- and S-centered radicals shows that photolysis cleaves the B–S bond. Furthermore, no radical other than NHC–boryl (from monosulfides), NHC–thioboryl (from bis-sulfides) or thiyl was observed. This supports a selective cleavage of the B–S bond.

All spectra are the sum of signals from the NHC–boryl or NHC–thioboryl radical adducts and the thiyl radical adduct in varied proportion. The respective contribution of each species to the ESR signal derives from the relative rates of addition of the radicals issued from the homolysis to the nitron. The rate of addition of NaphthylS[•] to PBN is probably so slow that only the B[•]-adduct was observed from **12**.

We also only observed one set of hyperfine coupling constants in the case of adducts with a stereogenic boron atom (all adducts from NHC–boryl bis-sulfides). This may mean that the addition to the nitron is stereoselective or, perhaps more likely, that two diastereomers with similar EPR spectra are formed.

Laser Flash Photolysis (LFP) Experiments. The kinetic aspects of the photolysis of the NHC–boryl sulfides were studied by LFP. NHC–boryl monosulfide **7** was irradiated at 355 nm under nitrogen, and the decay of the absorbance was observed at 450 nm (Figure 5A, curve a). One transient appeared to result. However, shape of the decay observed under air revealed the presence of two transients and hence two intermediates. One intermediate was quenched by oxygen at a rate near diffusion control ($k_{O_2} \approx 5 \times 10^9$ M⁻¹ s⁻¹, Figure 5A,

Table 2. ESR Parameters Characterizing the NHC–Boryl/PBN Radical Adducts Observed for the Photolysis of the Different NHCB–Boryl Sulfides^c

Entry	Substrate	Adduct	Hfc (G)			
			aN	aH	aB	
1	4		21•	15.1	2.1	4.6
2	11		24•	15.2	2.7	4.4
3 ^a	12		26•	15.2	2.7	4.4
4	5		28•	15.1	2.7	4.2
5	7		29•	15.1	2.7	4.2
6	8		29•	15.1	2.7	4.2
7 ^b	13		30•	15.2	2.8	4.4
8 ^a	14		31•	15.2	3.1	4.2
9	16		32•	15.2	3.0	4.3
10 ^a	17		33•	15.2	3.0	4.2

^aAr = 2-naphthyl. ^bAr = *p*-MeO-C₆H₄. ^cHfc = hyperfine coupling constant.

curve b). This intermediate has a short lifetime (~100 ns) when oxygen is present. The remaining transient has a maximum absorption at 450 nm that is not affected by oxygen (Figure 5B). So the other intermediate has a long lifetime (>5 μs).

The LFP observations again show that the photoirradiation of 7 generates two radicals. Based on the ESR experiments, we identify them as the NHC–boryl and thiyl radicals obtained by B–S bond homolysis. Under air, the short-lived radical is the NHC–boryl radical, which is known to react with oxygen at diffusion control.⁸ The long-lived species is the thiyl radical,

Scheme 1. Radicals Involved in the ESR-Spin Trap Spectra Obtained from 4, 11, and 12 (PBN Trap)

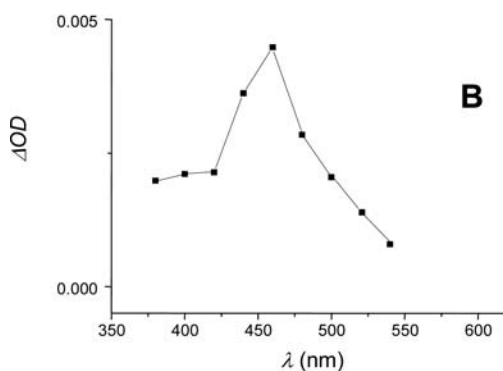
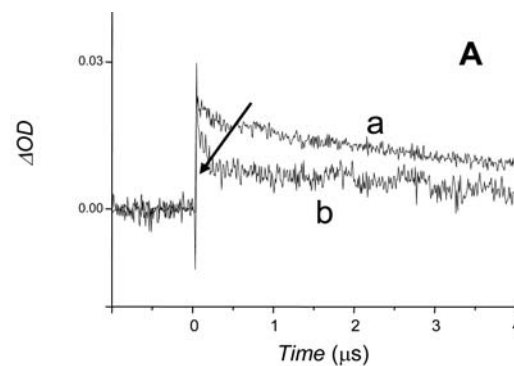
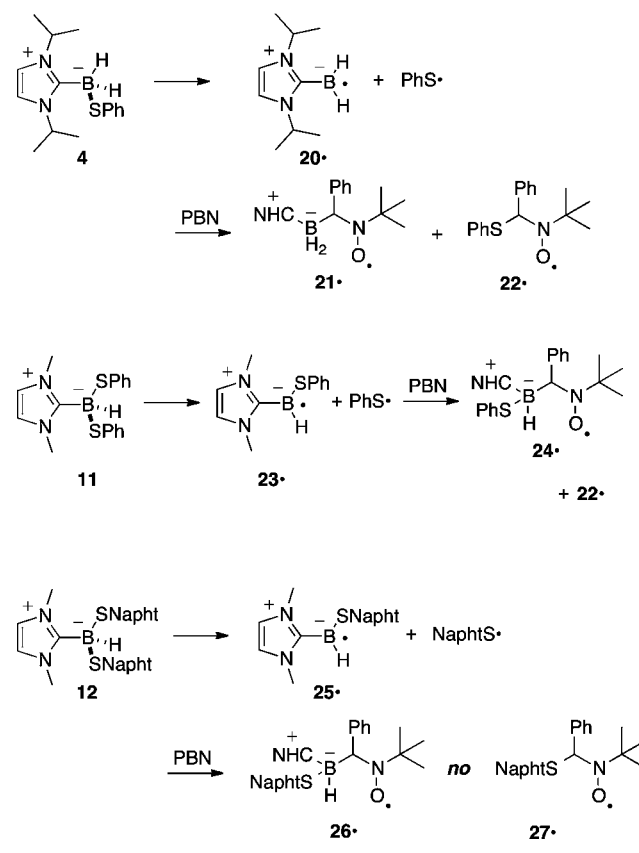


Figure 5. (A) Kinetics at 450 nm after laser excitation at 355 nm of 7 (a) under nitrogen and (b) under air and (B) spectrum recorded for $t = 3 \mu\text{s}$ under air (OD = optical density).

which has an absorbance at 450 nm and reacts only very slowly with oxygen.³¹ Under nitrogen, the NHC–boryl radical lives much longer. Its decay thus cannot be separated from that of the thiyl radical since both absorb at 450 nm.

The rising time for all transient species under laser excitation is less than 30 ns (within the resolution time of our LFP setup), which means that the dissociation rate constant for the B–S bond is very high ($k_{\text{diss}} > 3.3 \times 10^7 \text{ s}^{-1}$). This also means that the cleavage of the B–S bond in the excited state is very efficient. Overall, the spin trapping and LFP experiments agree nicely.

Molecular Orbital Calculations. To better understand the photochemical behavior, the B–S cleavage was investigated by using molecular orbitals calculations. The calculations of both HOMO and LUMO of **11** were performed first at the UB3LYP/6-31G* level (Figure 6). The HOMO exhibits a σ

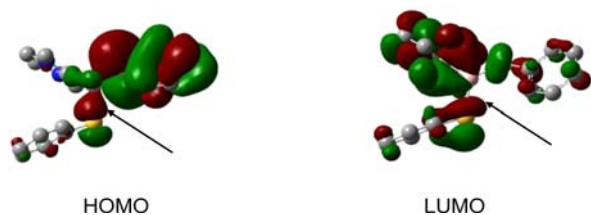


Figure 6. HOMO and LUMO for **11** at UB3LYP/6-31G* level; the σ and σ^* characters are indicated by arrows.

character, whereas the LUMO clearly shows a σ^* character for the B–S bond. Therefore, excitation of the NHC–boryl sulfide populates an antibonding orbital and can lead to bond cleavage.

A long-range correlated functional (CAM-B3LYP³²) was used to calculate the excited triplet state of NHC–boryl monosulfide **4**, and the results were compared with those obtained with the B3LYP functional. The transition state (TS) for the B–S cleavage in **4** from its lowest excited triplet state was located using the QST2 approach (synchronous transit-guided quasi-Newton (STQN) method) at both UB3LYP/6-31G* and CAM-B3LYP/6-31G* levels. The B–S bond lengths found in the transition states were 2.2 and 2.26 Å, respectively (Figure 7A).

The potential energy surface for the triplet state cleavage was also calculated for **4** to better understand this cleavage process. To do so, the geometry of the triplet state was fully optimized while constraining the B–S bond lengths with increasing values. The potential energy showed a maximum at about 2.15–2.2 Å (B3LYP) and 2.25 Å (CAM-B3LYP, Figure 7B). These results are in excellent agreement with the QST2 calculations. Similar results were obtained for the 6-31G* and 6-311G* basis sets (Figure 7B). An increasingly important stabilization was observed for increasing B–S bond lengths for both functionals. This is expected for a dissociative character for T_1 . The cleavage is also highly exothermic ($>12 \text{ kcal mol}^{-1}$)

The barrier determined with B3LYP is slightly lower than that found with CAM-B3LYP ($<1 \text{ kcal mol}^{-1}$ vs. $\sim 4 \text{ kcal mol}^{-1}$). This lower barrier with B3LYP is consistent with the difficulty to fully optimize the triplet state of **4** at the UB3LYP/6-31G* level. The minimum optimized structure using the latter functional does not correspond to a single molecule structure but to the two radicals released by the bond cleavage.

However, the barriers for the B–S cleavage for both functionals were similar to or lower than those found for the cleavage of the excited triplet state of the common and

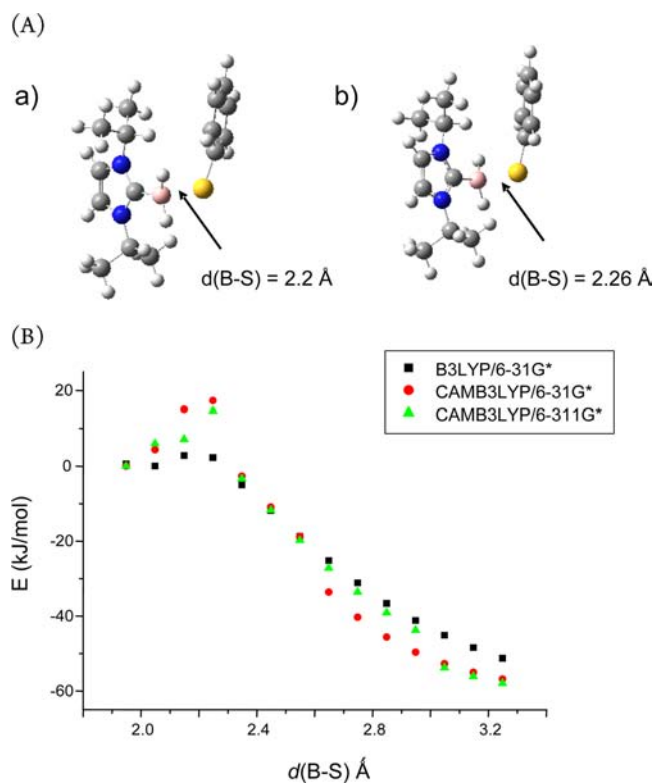


Figure 7. (A) TS structures found for the cleavage of **4** at (a) B3LYP/6-31G* and (b) CAM-B3LYP/6-31G* levels (QST2 approach) and (B) potential energy surfaces for the triplet state of **4** at increasing fixed B–S length at UB3LYP/6-31G* (black squares), CAM-B3LYP/6-31G* (red circles), and CAM-B3LYP/6-311G* (green triangles) level.

extremely efficient type I photoinitiator 2,2-dimethoxy-2-phenylacetophenone (DMPA, $4.5 \text{ kcal mol}^{-1}$).³³ This is in agreement with an efficient cleavage process for the NHC–boryl sulfides.

These calculations correlate also well with the low calculated BDEs for the B–S bonds in NHC–boryl sulfides (47–60 kcal/mol, Table 1). The BDEs are again in the range of those of other cleavable photopolymerization photoinitiators. For example, the C–C BDE is approximately 55 kcal/mol for 2,2-dimethoxy-2-phenylacetophenone.³³

Sensitized B–S Cleavage. The NHC–borosulfide compounds have a significant UV absorption at rather short wavelengths ($\lambda < 330 \text{ nm}$, Table 1). Therefore, it would be interesting to achieve the photolysis by using a less energetic, longer wavelength. Sensitization offers such an opportunity. Monosulfide **4** was again chosen as representative NHC–boryl sulfide. Benzophenone (BP) and 2-isopropylthioxanthene-9-one (ITX) have photochemical properties suitable for the generation of NHC–boryl and thiyl radicals with an irradiation source wavelength above 340 nm.

In a typical photosensitization experiment, a solution of BP (or ITX) and **4** in *tert*-butylbenzene was irradiated at $\lambda > 340 \text{ nm}$ in the presence of PBN, and the formation of nitroxide adduct radicals was followed by ESR spectroscopy. Two nitroxide radical adducts were observed with $a_N = 15.1$, $a_H = 2.2$, and $a_B = 4.6 \text{ G}$ and $a_N = 13.9$ and $a_H = 2.0 \text{ G}$ (Figure 8). These values match the data for NHC–boryl and phenylthiyl radical nitroxide adducts, respectively (see above). A control

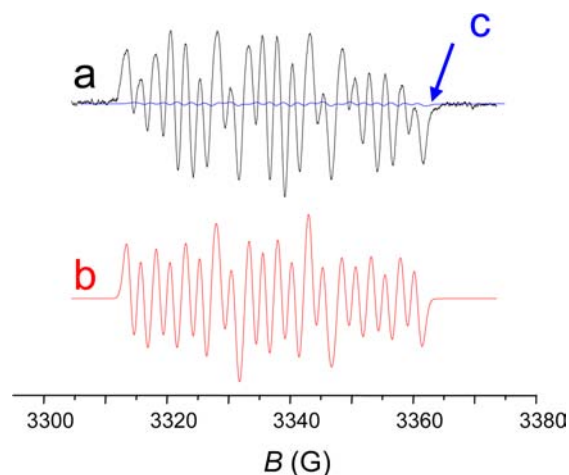


Figure 8. ESR-spin trapping spectra for the irradiation of a BP/4 solution in *tert*-butylbenzene ([BP] = 0.04 M; [4] = 0.02 M; [PBN] = 0.01 M), experimental (a) and simulated (b) spectra; (c) experimental ESR-spin trapping spectrum for the irradiation of a 4 solution in *tert*-butylbenzene ([4] = 0.02 M; [PBN] = 0.01 M).

experiment in the absence of benzophenone showed only a very weak signal (compare curves a and c in Figure 8).

The low production of radicals in the absence of sensitizer shows that the sensitizer absorbs most of the photon energy at the wavelength used. The rate constants for the sensitized processes were determined by laser flash photolysis by following the decay of the signals of ^3ITX and ^3BP . The rate constants for the $^3\text{ITX}/4$ and $^3\text{BP}/4$ interactions in toluene were found to be 10^8 and $2 \times 10^9 \text{ M}^{-1} \text{ s}^{-1}$, respectively (Figure 9A). The residual absorption is maximum at about 450 nm and a minor absorption for $\lambda \approx 540 \text{ nm}$ was also observed (Figure 9B).

These LFP results are in agreement with a triplet–triplet type sensitization (eqs 1a and 1b). The residual absorption is in

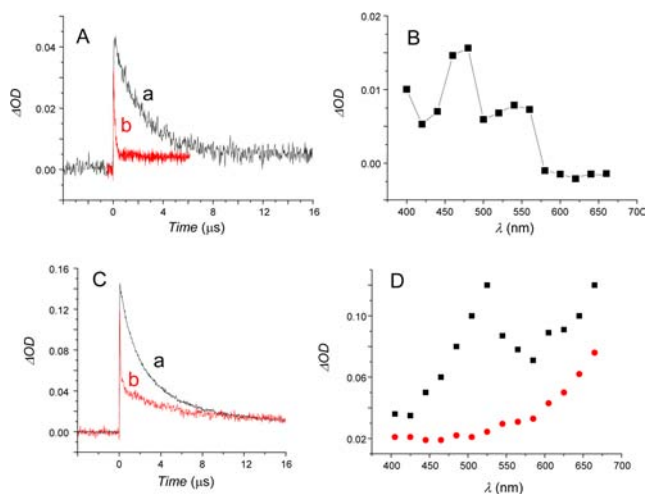
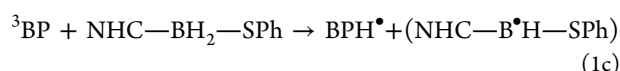
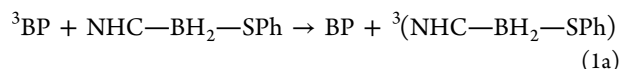
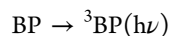
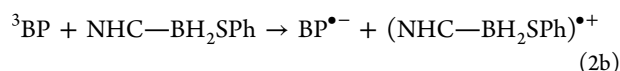
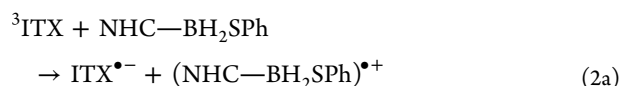


Figure 9. (A) kinetics at 525 nm after laser excitation at 355 nm of (a) benzophenone and (b) benzophenone/4 ([4] = 0.0036 M) under N_2 in toluene, (B) spectrum recorded for $t = 5 \mu\text{s}$ for the excitation of the benzophenone/4 solution in toluene, (C) kinetics at 525 nm after laser excitation at 355 nm of (a) benzophenone and (b) benzophenone/4 ([4] = 0.0036 M) in acetonitrile, and (D) spectrum recorded for $t = 50 \text{ ns}$ (squares) and $2 \mu\text{s}$ (circles) for the laser excitation of the BP/4 solution in acetonitrile.

agreement with the reported spectrum of PhS^\bullet (Figure 9B, see also Figure 5) and is consistent with the ESR data. The minor absorption is ascribed to the ketyl radical of benzophenone, potentially arising from a hydrogen abstraction from the remaining B–H bonds in 4 (eq 1c). The latter reaction is known for NHC– BH_3 complexes, and it is at the root of their behavior as type II co-initiators for free-radical photopolymerizations.⁷



Higher rate constants for the disappearance of the sensitizer triplet states were found in acetonitrile, a polar solvent. The rate for the $^3\text{ITX}/4$ interaction was $1.1 \times 10^9 \text{ M}^{-1} \text{ s}^{-1}$ and that of the $^3\text{BP}/4$ interaction was $6 \times 10^9 \text{ M}^{-1} \text{ s}^{-1}$ (Figure 9C). In this case, however, the residual absorption for the product of reaction of ^3BP or ^3ITX with 4 peaked for $\lambda > 650 \text{ nm}$ (Figure 9D). This absorption was ascribed to either $\text{BP}^{\bullet-}$ or $\text{ITX}^{\bullet-}$. These radical anions were not observed in the apolar solvent (compare Figure 9, panels B and D). This behavior suggests that a competitive electron transfer pathway exists in polar media (eqs 2).



Electrochemical Properties. To assess the potential of electrochemical activation of the B–S bond and to support the suggested electron transfer of eqs 2a and 2b, we carried out voltammetric measurements in acetonitrile (+ 0.1 M *n*- Bu_4BF_4) at a millimetric carbon electrode with NHC–boryl sulfides 1–3 and 11–13.

Reduction. No reduction wave was observed for 1, 3, 11, or 13 indicating that the B–S bond is resistant to cleavage at the electrode, despite its relative weakness. This is in contrast to the behavior of NHC– BH_2I complexes, which accept one electron to give the corresponding boryl radicals NHC–BH_2^\bullet (peak potential close to -2.5 V vs. SCE at low scan rate).¹⁸

However, a one-electron irreversible wave peaking at -2.52 V vs. SCE ($\nu = 0.2 \text{ V/s}$) was observed for compounds bearing *S*-naphthyl substituents, such as NHC–boryl monosulfide 2 (Figure 10a). NHC–boryl bis-sulfide 12 showed two closely located irreversible reduction waves peaking at -2.43 and -2.53 V vs. SCE (Figure 10b). The latter is a one-electron wave identical to the reduction wave of 2, while the former is a two-electron wave, leading to the formation of 2 through the cleavage of one B–S bond. The reduction of 2 delivers NHC–BH_2^\bullet and naphthyl thiolate (naphthS^-). The B–S bond cleavage was confirmed by the observation of the oxidation wave of naphthS^- when the potential was scanned at positive values after reduction. The latter wave was identified by comparison with an authentic sample (obtained from the deprotonation of 2-naphthalenethiol).

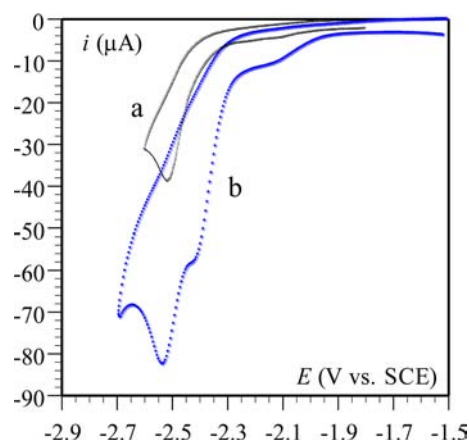
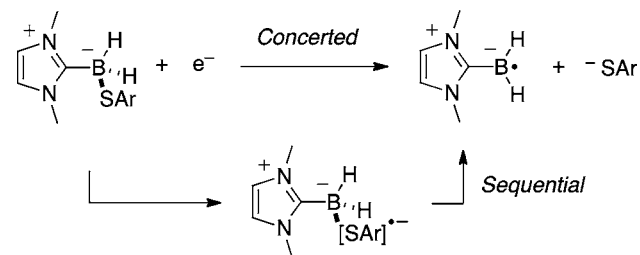


Figure 10. Cyclic voltammetry of NHC–boryl sulfides (1 mM in acetonitrile + 0.1 M *n*-Bu₄NBF₄, $\nu = 0.1$ V/s) at a glassy carbon electrode (3 mm diameter): (a, black) **2**. (b, blue) **12**.

To explain these observations we considered the two possible mechanisms for the reductive cleavage of a bond involving a heavy atom.^{34,35}

First, a two-step mechanism may be followed (Scheme 2, bottom). In this case, the electron is first transferred to a low-

Scheme 2. Concerted (top) and Sequential (bottom) Pathways for the One Electron Reductive Cleavage of NHC–Boryl Sulfides



lying orbital (e.g., a π^* orbital in an aromatic compound), before being transferred into the σ^* orbital of the bond being broken. In the cases of **1**, **3**, **11**, and **13**, no such accommodating π^* orbital exists because the orbital located on the phenyl substituent is too high in energy, thus preventing this reduction pathway.

A second possibility is a concerted reaction (Scheme 2, top), in which electron transfer and bond breaking occur in the same elementary step through one single transition state. Such a mechanism is favored by low bond dissociation energy, since the major contribution to the activation barrier derives from the bond cleavage. More precisely, it has been established that the activation–driving force relationship for the reaction $R-X + e^- \rightarrow R^\bullet + X^-$ may be expressed by eq 3 where D_{RX} is the homolytic dissociation energy of the R–X bond and λ_0 the solvent reorganization energy.³⁴

$$\Delta G^\ddagger = \frac{D_{RX} + \lambda_0}{4} \left(1 + \frac{\Delta G^\circ}{D_{RX} + \lambda_0} \right)^2 \quad (3)$$

The standard free energy of the reaction leading to complete dissociation (E , electrode potential; $E_{RX/R^\bullet + X^-}^\circ$, standard potential of the R–X/R $^\bullet$ + X $^-$ couple) is given by eq 4,

where ΔS° is the bond dissociation entropy (usually small) and E_{X^\bullet/X^-}° the standard potential of the X $^\bullet$ /X $^-$ redox couple.

$$\begin{aligned} \Delta G^\circ &= F(E - E_{RX/R^\bullet + X^-}^\circ) \\ &= F(E + D_{RX} - T\Delta S^\circ - E_{X^\bullet/X^-}^\circ) \end{aligned} \quad (4)$$

From eqs 3 and 4, it appears that the free energy barrier ΔG^\ddagger for the reaction depends on D_{RX} but also on the standard redox potential of the leaving group E_{X^\bullet/X^-}° , involving in our case the redox couple ArS $^\bullet$ /ArS $^-$ (Ar = phenyl with **1** and **11**, Ar = *p*-methoxyphenyl with **3** and **13**, Ar = 2-naphthyl with **2** and **12**). If the homolytic bond dissociation energy is small but E_{X^\bullet/X^-}° is not positive enough, then the activation energy becomes large due to unfavorable thermodynamics (ΔG° being not very negative) and the reaction is severely slowed. This is what likely happens with NHC–boryl sulfides **1**, **3**, **11**, and **13**.

The reaction becomes even more unfavorable with **2**, since in this case the leaving group is a naphthyl thiolate, whose E_{X^\bullet/X^-}° is even less positive than those of **1**, **3**, **11**, and **13**. However, an irreversible one-electron wave was observed for **2**. This wave is thin (midpeak width close to ca. 70 mV), which is characteristic of an E + C sequential process, where the electron transfer step (E) is followed by a fast, irreversible chemical reaction (C).³⁵ With this compound, the naphthyl substituent has its π^* orbital partially delocalized onto the sulfur through its nonbonding electron pair and can accommodate the extra electron before the bond is broken better than a phenyl group. With **12**, the naphthyl substituents also provide accessible orbitals for the reduction process to occur. In this case, one of the B–S bonds is cleaved on the first cathodic wave, leading to **2**, which goes on to be reduced on the second, more negative wave.

Overall, the NHC–boryl sulfides are difficult to reduce at an electrode, necessitating highly aromatic thiolate leaving groups and very negative potentials.

Oxidation. Compounds **2**, **4**, **12**, and **13** give rise to a moderately positive peak-shaped oxidation wave (+1.01 V vs. SCE at 0.5 V·s $^{-1}$ for **4**, +0.91 V vs. SCE at 0.1 V·s $^{-1}$ for both **2** and **12**, and +0.77 V vs. SCE at 0.5 V·s $^{-1}$ for **13**, Figure 11). The reduction waves of naphthyl disulfide in the case of **2** and **12** and *p*-methoxyphenyl disulfide in the case of **13** were identified after scanning the potential at negative values after oxidation. This was obtained by comparison with the reduction voltammograms of authentic samples of the disulfides.

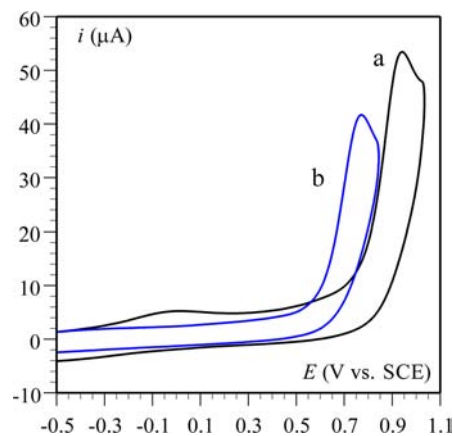


Figure 11. Cyclic voltammetry of NHC–boryl sulfides (1 mM in acetonitrile + 0.1 M *n*-Bu₄NBF₄, $\nu = 0.5$ V/s) at a glassy carbon electrode (3 mm diameter): (a, black) **12**; (b, blue) **13**.

The previous observations show that the oxidation waves corresponds to the oxidative cleavage of the B–S bonds. The resulting radical cation likely fragments to the NHC–boronium³⁶ and sulfur centered radical since the presence of the disulfides in the electrochemical vessel can only be explained by the dimerization of the thiyl radicals.

The values obtained for the oxidation potentials are compatible to the photo-oxidation observed previously. By using a reduction potential of -1.79 V for BP and a triplet state energy of 2.98 eV for BP, one can estimate a reduction potential of 1.19 V for ³BP, largely positive as compared with the experimental oxidation peaks.

Application to Free Radical Photopolymerizations.

We have previously shown that photogenerated NHC–boryl radicals initiate free-radical polymerizations of acrylates in the presence of oxygen.⁸ We thus decided to investigate the possibility of applying the new photogeneration of NHC–boryl radicals to direct and sensitized photopolymerizations. In the former case, NHC–boryl sulfides would be type I photoinitiators.

All the borane-based co-initiators that we have introduced thus far rely on a hydrogen atom transfer from the corresponding NHC–boranes directly to an excited state of benzophenone in type II photoinitiations^{7,9} or to radicals derived from known type I systems.⁶ However, directly cleavable structures generating NHC–boryl radicals remained unknown. Thus, having a family of NHC–borane-based initiating systems for standard and sensitized type I photopolymerizations would fill the remaining gaps in the NHC–boryl radical initiated photopolymerization of acrylates.

Type I systems are attractive because they do not suffer from competitive quenching of the excited state of the photoinitiator by the monomer. This quenching can prevent an efficient hydrogen abstraction reaction from the co-initiators. Besides, type II systems can be associated with low yields in radicals because of deleterious back electron or hydrogen transfer reactions between the hydrogen donor (co-initiator) and the photoinitiator.³³

We selected trimethylolpropane triacrylate (TMPTA) as our benchmark monomer for testing the NHC–boryl sulfides. Its photopolymerization is monitored by the disappearance of the IR signal associated with the C=C double bond. TMPTA is a trifunctional acrylate, so it leads to cross-linking. The polymerization curves have a typical exponential shape. They flatten at higher conversion because the geometrical constraints associated with the cross-linking and the change of the reaction medium physical aspect from solution to hard and glassy prevents the full consumption of the alkenes (Figure 12).

Type I Photopolymerization. In a typical polymerization, irradiation of TMPTA with a UV lamp in the presence of NHC–boryl bis-sulfide **11** led to rapid polymerization (Figure 12, curve a), whereas no polymerization was observed in absence of **11** (Figure 12, curve b). The final conversions reached and polymerization rates of all the investigated compounds are gathered in Table 3 (Figure S4, Supporting Information).

The polymerization photoinitiation has three stages that contribute to the polymerization rate: (i) the light absorption properties of the various molecules present; (ii) the quantum yield of the B–S bond cleavage; (iii) the addition rate of the generated radicals (NHC–boryls and thiyls) onto acrylates. The interplay among these parameters accounts for the

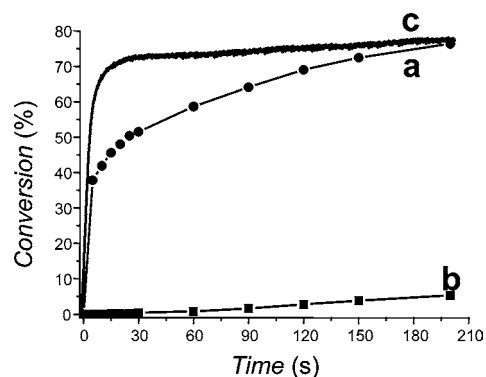


Figure 12. Photopolymerization profiles of TMPTA upon Xe–Hg lamp irradiation ($\lambda > 300$ nm) in laminate (a) in the presence of **11** (2% w/w), (b) in the absence of **11**, and (c) in the presence of 2,2-dimethoxy-2-phenylacetophenone (DMPA) (2% w/w).

Table 3. Polymerization Rates (R_p) and Final Conversion for the Polymerization of TMPTA upon Xe–Hg Lamp Exposure (NHCBS Photoinitiator 2% w/w)^a

entry	NHCBS (mono)	$R_p/[M]_0 \times 100$ (s^{-1})	conv. (%)	entry	NHCBS (di)	$R_p/[M]_0 \times 100$ (s^{-1})	conv. (%)
1	2	14.7	76	10	11	7	77
2	3	20.5	69	11	12	9.2	69
3	4	13.5	72	12	13	13	71
4	5	8.6	73	13	14	6.5	72
5	6	17.1	68	14	15	6.3	69
6	7	9	68	15	16	7.8	64
7	8	14.6	74	16	17	3.4	64
8	9	13.4	73	17	18	18.4	71
9	10	13.7	71	18	19	9	63

^a $[M]_0$ is the initial monomer concentration.

variations observed, but it is difficult to deconvolute the effects to have a predictive structure/activity relationship.

DMPA absorbs more energy (I_{abs}) than NHC–boryl sulfides. For example, DMPA has a 12-fold calculated I_{abs} relative to **11** for the selected Xe–Hg lamp.³⁷ Because the polymerization rate R_p is proportional to the square root of $I_{abs}\Phi_I$ (where Φ_I is the initiation quantum yield), the polymerization is more rapid with DMPA (Figure 12).

Sensitized Type I Photopolymerization. The NHC–boryl sulfides absorb light only weakly above 330 nm; a rather energetic photon is used in this polymerization. We have shown that the B–S bond cleavage can be achieved with higher wavelength light in low polarity media by using a sensitizer (eqs 1a and 1b). Thus, we examined whether the sensitizer would help initiate the photopolymerization at a longer wavelength.

We devised a series of experiments in which an aromatic ketone (2-isopropylthioxanthone, ITX) was selected as sensitizer. This compound exhibits excellent light absorption properties ($\lambda_{max} \approx 375$ nm with an extinction coefficient well above 5000 $M^{-1} cm^{-1}$), and the TMPTA acrylate matrix is a relatively low polarity medium. It should be compatible with the sensitized formation of the radicals but not with the electron transfer (see above). All photopolymerizations were carried out in a vessel open to air.

For $\lambda > 340$ nm, NHC–boryl monosulfide **4** alone does not lead to polymerization (Figure 13, curve a), while ITX alone is not very efficient (Figure 13, curve b). The ITX/**4** system,

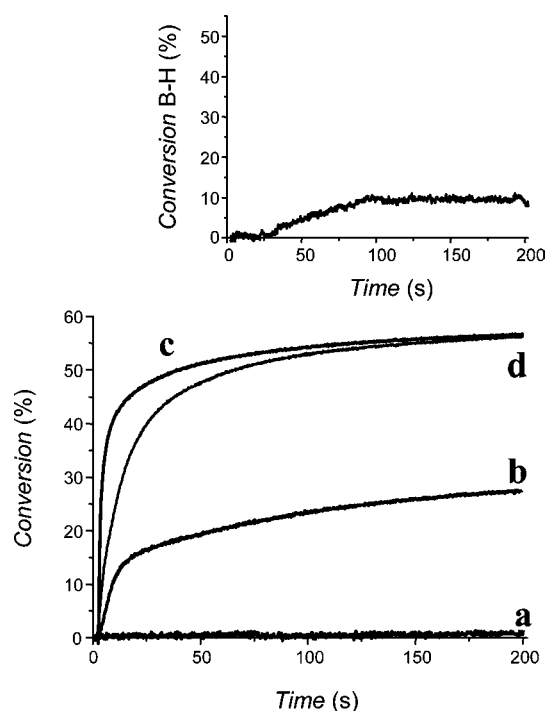


Figure 13. Photopolymerization profiles of TMPTA upon a Xe–Hg lamp irradiation ($\lambda > 340$ nm) under air for different photoinitiating systems: (a) **4** (2% w/w); (b) 2-isopropylthioxanthone (1% w/w); (c) 2-isopropylthioxanthone/**4** (1%/2% w/w); (d) 2-isopropylthioxanthone/**11** (1%/2% w/w). Inset, B–H conversion in profile c.

however, leads to an efficient polymerization process (Figure 13, curve c). ITX/NHC–boryl disulfide **11** also led to a smooth polymerization (Figure 13, curve d).

That **4** alone is not an efficient photoinitiator is a direct consequence of its lack of absorption in the spectral range considered. The excited ITX does abstract a hydrogen atom from NHC–boranes, and the NHC–boryl sulfides have one or two hydrogen atoms. The abstraction of any of these atoms might lead to the polymerization of TMPTA through a type II mechanism. We do not think this happens here for the following reasons: (i) The rate of the sensitized B–S bond cleavage (see above) is 10–60 times faster than that of the hydrogen atom transfer from the B–H bond in NHC–boranes to the excited state of the sensitizer.⁹ So it is unlikely that the polymerization would follow the slower hydrogen abstraction path. (ii) The LFP spectrum of the laser excitation of the benzophenone/**4** solution in acetonitrile shows an absorption at 450 nm that is not quenched by dioxygen. This indicates the presence of thiyl radicals rather than the NHC–boryl radicals that would arise from H abstraction. Caution must be exercised because the latter would be NHC–B(\bullet)(H)SAr, which could not be characterized by LFP. However, the presence of thiyl radicals can only be explained by the dissociative mechanism. (iii) The ESR spin trapping experiments also show the presence of thiyl radicals (see above). (iv) Consumption of the B–H bond during the polymerization is very low (<10%; inset in Figure 13). On the contrary, the B–H bond disappearance closely followed the conversion in the regular type II polymerization we have carried out (benzophenone/NHC–BH₃ initiating system). In addition, it is also likely that at least some B–H conversion in the inset should be ascribed to the H transfer to the polarly matched thiyl radicals formed during the

reaction,^{3,6} thus making the B–H cleavage via a type II transfer even less likely.

Furthermore, thiyl radicals can start the polymerization of acrylates; however, the efficiency is low because thiyl radicals are electrophilic and polarly mismatched with the electron-poor acrylates. Therefore, their addition rate to acrylate monomers is relatively low.³³ Finally, all the sensitized photopolymerizations proceed under air, which shows that the NHC–boryl sulfides retain the properties of the NHC–boranes⁸ also for type I mechanisms.

CONCLUSIONS

The B–S bond in NHC–boryl mono- or bis-sulfides can be cleaved homolytically to NHC–boryl or NHC–thioboryl radicals and thiyl radicals by using light. UV irradiation at about 300 nm leads to direct cleavage of the bond, while use of a sensitizer leads to bond cleavage at a longer wavelength. In contrast, the electrochemical reductive cleavage of the B–S bond is difficult, and photocleavage is the method of choice for generating the boryl radicals in this class of molecules.

The easy photolytic cleavage of the B–S bond makes the NHC–boryl sulfides good type I photopolymerization initiators for the polymerization of acrylates under air. NHC–boranes can thus promote both type I and type II photopolymerizations, as well as act as additives to improve the polymerization efficiency.

Further work will seek to design more efficient light-absorbing and visible-light photoinitiators, as well as to extend the applications of NHC–boryl sulfides to synthetic organic chemistry.

ASSOCIATED CONTENT

Supporting Information

Materials and methods, UV and ESR-spin trapping spectra, photolysis, polymerization profiles, and Z-matrices. This material is available free of charge via the Internet at <http://pubs.acs.org>.

AUTHOR INFORMATION

Corresponding Authors

robert@univ-paris-diderot.fr
emmanuel.lacote@univ-lyon1.fr
jacques.lalevee@uha.fr

Notes

The authors declare no competing financial interest.

ACKNOWLEDGMENTS

This work was supported by the French Agence Nationale de Recherche (Grant ANR-11-BS07-008, NHCX), UHA, ENSC-Mu, CPE Lyon, Université de Lyon, Université Paris Diderot, the Institut Universitaire de France (IUF), the US National Science Foundation, and CNRS. E.L. thanks Actelion and ENSCMu for the Actelion award.

REFERENCES

- Curran, D. P.; Solovyev, A.; Makhlof Brahmi, M.; Fensterbank, L.; Malacria, M.; Lacôte, E. *Angew. Chem., Int. Ed.* **2011**, *50*, 10294–10317.
- Ueng, S.-H.; Makhlof Brahmi, M.; Derat, E.; Fensterbank, L.; Lacôte, E.; Malacria, M.; Curran, D. P. *J. Am. Chem. Soc.* **2008**, *130*, 10082–10083.
- Pan, X.; Lacôte, E.; Lalevée, J.; Curran, D. P. *J. Am. Chem. Soc.* **2012**, *134*, 5669–5674.

- (4) Chu, Q. L.; Makhlof Brahmī, M.; Solovyev, A.; Ueng, S.-H.; Curran, D.; Malacria, M.; Fensterbank, L.; Lacôte, E. *Chem.—Eur. J.* **2009**, *15*, 12937–12940.
- (5) (a) Lindsay, D. M.; McArthur, D. *Chem. Commun.* **2010**, *46*, 2474–2476. (b) Horn, M.; Mayr, H.; Lacôte, E.; Merling, E.; Deaner, J.; Wells, S.; McFadden, T.; Curran, D. P. *Org. Lett.* **2012**, *14*, 82–85.
- (6) Lalevée, J.; Telitel, S.; Tehfe, M. A.; Fouassier, J. P.; Curran, D. P.; Lacôte, E. *Angew. Chem., Int. Ed.* **2012**, *51*, 5958–5961.
- (7) Tehfe, M. A.; Makhlof Brahmī, M.; Fouassier, J. P.; Curran, D. P.; Malacria, M.; Fensterbank, L.; Lacôte, E.; Lalevée, J. *Macromolecules* **2010**, *43*, 2261–2267.
- (8) Tehfe, M. A.; Monot, J.; Makhlof Brahmī, M.; Bonin-Dubarle, H.; Curran, D. P.; Malacria, M.; Fensterbank, L.; Lacôte, E.; Lalevée, J.; Fouassier, J. P. *Polym. Chem.* **2011**, *2*, 625–631.
- (9) Tehfe, M. A.; Monot, J.; Malacria, M.; Fensterbank, L.; Fouassier, J. P.; Curran, D. P.; Lacôte, E.; Lalevée, J. *ACS Macro Lett.* **2012**, *1*, 92–95.
- (10) Telitel, S.; Schweizer, S.; Morlet-Savary, F.; Graff, B.; Tschamber, T.; Blanchard, N.; Fouassier, J. P.; Lelli, M.; Lacôte, E.; Lalevée, J. *Macromolecules* **2012**, *46*, 43–48.
- (11) Kyne, S. H.; Aitken, H. M.; Schiesser, C. H.; Lacôte, E.; Malacria, M.; Ollivier, C.; Fensterbank, L. *Org. Biomol. Chem.* **2011**, *9*, 3331–3337.
- (12) Pan, X.; Vallet, A.-L.; Schweizer, S.; Dahbi, K.; Delpech, B.; Blanchard, N.; Graff, B.; Geib, S. J.; Curran, D. P.; Lalevée, J.; Lacôte, E. *J. Am. Chem. Soc.* **2013**, *135*, 10484–10491.
- (13) Ueng, S.-H.; Solovyev, A.; Yuan, X. T.; Geib, S. J.; Fensterbank, L.; Lacôte, E.; Malacria, M.; Newcomb, M.; Walton, J. C.; Curran, D. P. *J. Am. Chem. Soc.* **2009**, *131*, 11256–11262.
- (14) Walton, J. C.; Makhlof Brahmī, M.; Monot, J.; Fensterbank, L.; Malacria, M.; Curran, D. P.; Lacôte, E. *J. Am. Chem. Soc.* **2011**, *133*, 10312–10321.
- (15) Wang, Y.; Quillian, B.; Wei, P.; Wannere, C. S.; Xie, Y.; King, R. B.; Schaefer, H. F.; Schleyer, P. v. R.; Robinson, G. H. *J. Am. Chem. Soc.* **2007**, *129*, 12412–12413.
- (16) Braunschweig, H.; Dewhurst, R. D.; Hammond, K.; Mies, J.; Radacki, K.; Vargas, A. *Science* **2012**, *336*, 1420–1422.
- (17) Braunschweig, H.; Chiu, C.-W.; Radacki, K.; Kupfer, T. *Angew. Chem., Int. Ed.* **2010**, *49*, 2041–2044.
- (18) Monot, J.; Solovyev, A.; Bonin-Dubarle, H.; Derat, E.; Curran, D. P.; Robert, M.; Fensterbank, L.; Malacria, M.; Lacôte, E. *Angew. Chem., Int. Ed.* **2010**, *49*, 9166–9169.
- (19) Matsumoto, T.; Gabbai, F. P. *Organometallics* **2009**, *28*, 4252–4253.
- (20) McArthur, D.; Butts, C. P.; Lindsay, D. M. *Chem. Commun.* **2011**, *47*, 6650–6652.
- (21) Farrell, J. M.; Hatnean, J. A.; Stephan, D. W. *J. Am. Chem. Soc.* **2012**, *134*, 15728–15731.
- (22) Monot, J.; Makhlof Brahmī, M.; Ueng, S.-H.; Robert, C.; Desage-El Murr, M.; Curran, D. P.; Malacria, M.; Fensterbank, L.; Lacôte, E. *Org. Lett.* **2009**, *11*, 4914–4917.
- (23) Bissinger, P.; Braunschweig, H.; Kraft, K.; Kupfer, T. *Angew. Chem., Int. Ed.* **2011**, *50*, 4704–4707.
- (24) Curran, D. P.; Boussonnière, A.; Geib, S. J.; Lacôte, E. *Angew. Chem., Int. Ed.* **2012**, *51*, 1602–1605.
- (25) Braunschweig, H.; Dewhurst, R. D. *Angew. Chem., Int. Ed.* **2013**, *52*, 3574–3583.
- (26) Kleeberg, C.; Crawford, A. G.; Batsanov, A. S.; Hodgkinson, P.; Apperley, D. C.; Cheung, M. S.; Lin, Z.; Marder, T. B. *J. Org. Chem.* **2012**, *77*, 785–789.
- (27) Braunschweig, H.; Damme, A.; Dewhurst, R. D.; Kramer, T.; Kupfer, T.; Radacki, K.; Siedler, E.; Trumpp, A.; Wagner, K.; Werner, C. *J. Am. Chem. Soc.* **2013**, *135*, 8702–8707.
- (28) Lee, K.-s.; Zhugralin, A. R.; Hoveyda, A. H. *J. Am. Chem. Soc.* **2010**, *132*, 12766–12766.
- (29) Ito, O.; Matsuda, M. *Bull. Chem. Soc. Jpn.* **1984**, *57*, 1745–1749.
- (30) (a) Baban, J. A.; Marti, V. P. J.; Roberts, B. P. *J. Chem. Soc., Perkin Trans. 2* **1985**, 1723–1733. (b) Baban, J. A.; Marti, V. P. J.; Roberts, B. P. *J. Chem. Soc., Perkin Trans. 2* **1986**, 1607–1611.
- (31) Lalevée, J.; Morlet-Savary, F.; Roz, M. E.; Allonas, X.; Fouassier, J. P. *Macromol. Chem. Phys.* **2009**, *210*, 311–319.
- (32) Yanai, T.; Tew, D.; Handy, N. *Chem. Phys. Lett.* **2004**, *393*, 51–57.
- (33) Fouassier, J. P.; Lalevée, J. *Photoinitiators for Polymer Synthesis: Scope, Reactivity and Efficiency*; Wiley-VCH: Weinheim, Germany, 2012.
- (34) Costentin, C.; Robert, M.; Savéant, J.-M. *Chem. Phys.* **2006**, *324*, 40–56.
- (35) Houmam, A. *Chem. Rev.* **2008**, *108*, 2180–2237.
- (36) De Vries, T. S.; Prokofjevs, A.; Vedejs, E. *Chem. Rev.* **2012**, *112*, 4246–4282.
- (37) Lalevée, J.; El-Roz, M.; Morlet-Savary, F.; Graff, B.; Allonas, X.; Fouassier, J. P. *Macromolecules* **2007**, *40*, 8527–8530.